

# Spiral structure in nearby galaxies

## II. comparative analysis and conclusions

S. Kendall<sup>1</sup>, C. Clarke<sup>1\*</sup>, R. C. Kennicutt<sup>1</sup>

<sup>1</sup> *Institute of Astronomy, University of Cambridge, Madingley Road, Cambridge CB3 0HA*

submitted, accepted

### ABSTRACT

This paper presents a detailed analysis of two-armed spiral structure in a sample of galaxies from the Spitzer Infrared Nearby Galaxies Survey (SINGS), with particular focus on the relationships between the properties of the spiral pattern in the stellar disc and the global structure and environment of the parent galaxies. Following Paper I we have used a combination of Spitzer Space Telescope mid-infrared imaging and visible multi-colour imaging to isolate the spiral pattern in the underlying stellar discs, and we examine the systematic behaviours of the observed amplitudes and shapes (pitch angles) of these spirals. In general, spiral morphology is found to correlate only weakly at best with morphological parameters such as stellar mass, gas fraction, disc/bulge ratio, and  $v_{flat}$ . In contrast to weak correlations with galaxy structure a strong link is found between the strength of the spiral arms and tidal forcing from nearby companion galaxies. This appears to support the longstanding suggestion that either a tidal interaction or strong bar is a necessary condition for driving grand-design spiral structure. The pitch angles of the stellar arms are only loosely correlated with the pitch angles of the corresponding arms traced in gas and young stars. We find that the strength of the shock in the gas and the contrast in the star formation rate are strongly correlated with the stellar spiral amplitude.

**Key words:** galaxies:individual–galaxies:spiral–galaxies:structure–infrared:galaxies

### 1 INTRODUCTION.

This paper is the second of two detailing an observational study of spiral structure for galaxies in the *Spitzer* Infrared Nearby Galaxies Survey (SINGS - Kennicutt et al. (2003)). This work also builds directly on an earlier study of M81 presented in Kendall et al. (2008). In the first paper (Kendall et al. 2011, hereafter Paper I), the methods and results from individual galaxies were presented together with a comparison between those galaxies in which grand design spiral structure was detected and those that lacked such structure. In this paper we focus on the subset of 13 galaxies (henceforth the ‘detailed sample’) in which it has been possible to characterise the properties of the spiral structure in detail and present an analysis of any trends within this sample.

Observational results have been crucial to the advances in the study of spiral structure, and the launch of the *Spitzer* Space Telescope provided a new resource in its high quality infrared data. This paper aims to build on previous studies in the optical and infrared, and provides a new dataset against which numerical simulations of spiral structure can be tested.

There have been numerous observational studies of spiral structure, some key results are as follows: Schweizer (1976) anal-

ysed six galaxies using optical data to produce profiles of surface brightness against azimuth. From these data Schweizer concluded that there must be an old disc component in the spiral arms of each of the galaxies studied and that the spiral arms reach amplitudes as large as 30 per cent relative to the disc. Other studies have confirmed this result; the measured ratio of arm to disc mass varies with galaxy and the exact method and wavelength used, but as a rule the contrast between arm and inter-arm regions in the optical is in the range 20 to 100 per cent (e.g. Schweizer (1976); Elmegreen & Elmegreen (1984); Grosbøl et al. (2004)), with more recent studies suggesting that an upper limit of 40 to 50 per cent is appropriate in the majority of cases (note that contamination from star forming regions can cause this quantity to be over-estimated particularly in the early studies which used the *I* band rather than near infrared (NIR) data). The amplitude of spiral arms is potentially important since it might be expected to directly affect the global star formation rate (SFR) in the galaxy: larger contrasts between the stellar arm-interarm regions are expected to cause the gas to shock more strongly, become more dense, and thus increase the star formation (bearing in mind that according to the Kennicutt-Schmidt law (Kennicutt 1998), star formation varies as  $\Sigma^{1.4}$ .) This association between star formation and spiral structure would appear to be borne out in cases like M81 and M51, where the vast majority of star formation lies on well defined spiral arms. Some studies have at-

\* E-mail: cclarke@ast.cam.ac.uk

tempted to correlate the rates of star formation with the strength of the stellar spiral arms: for example, Cepa & Beckman (1990) found that star formation is triggered preferentially by spiral arms (with a ‘non-linear dependency’). Seigar & James (1998) found a link between SFR measured from far-infrared luminosity and  $K$  band arm strength, and found that the SFR increases with arm strength. Similarly, Seigar & James (2002) reported that the spiral arm strength (in  $K$ ) correlates with  $H\alpha$  (a SFR tracer) suggesting that stronger potential variations (and associated shocks) lead to a larger SFR (up to a limiting threshold, above which the SFR is constant). Nevertheless, the picture does not always appear to be this simple: studies of flocculent galaxies showing underlying  $m=2$  spiral structure in the mass density as traced by near infrared emission (Elmegreen et al. 1999, Thornley 1996) clearly show that star formation is not always preferentially located on two well defined spiral arms. More recently Elmegreen et al (2011) analysed NIR imaging for a sample of nearby galaxies from the Spitzer S<sup>4</sup>G survey (Sheth et al. 2010) and found that the distinctions between grand design and flocculent arm structures seen in the visible extend to the NIR structure as well.

Another property of spiral galaxies that has been extensively studied is the pitch angle (i.e. the angle between spiral features and the tangential direction): Kennicutt & Hodge (1982) measured pitch angles and compared them against theoretical predictions from both QSSS (quasi-stationary spiral structure - Lindblad 1964; Lin & Shu 1964, 1966) and SSPSF (stochastic self-propagating star formation - Mueller & Arnett 1976; Gerola & Seiden 1978) theories and found qualitative trends that were in agreement with both theories but poor detailed agreement in both cases. Similarly, Kennicutt (1981) compared pitch angle against RSA type (largely dependent on disc resolution), and found a good correlation on average, but with a large degree of scatter. A correlation between pitch angle,  $i$ , and bulge-to-disc ratio was also found, where a larger pitch angle (more open spiral pattern) is associated with a smaller bulge fraction; again there is a large scatter in the pitch angle at given bulge to disc ratio. In addition the maximum rotational velocity was found to correlate strongly with pitch angle, with galaxies with large rotational velocities having more tightly wound spirals.

However, there are indications that the appearance of spiral arms in the NIR and optical do not always correlate (an extreme case being the optically flocculent galaxies with NIR arms already noted above). Some studies using NIR data (e.g. Seigar & James (1998) have not found the same trends as Kennicutt. Block & Wainscoat (1991) found evidence that the spiral arms are less tightly wound in the NIR than the optical. Likewise, Block et al. (1994) compare the NIR and optical morphology for a sample of galaxies and, for a number of spirals, found significant differences between the pitch angles of the arms in the optical and NIR. They found that galaxies generally appear to be of an earlier Hubble type when viewed in the NIR ( $K'$  band) than in the optical, the traditional wavelength for such classifications. On the other hand, more recent studies have found a generally good agreement between the pitch angles measured in the NIR and B band (Seigar et al. 2006, Davis et al. 2012); in the few cases where the two values are significantly different, there is a mild preference for the NIR pitch angles to be larger. Turning now to correlations with galactic parameters, Seigar & James (1998) found no evidence of a correlation between NIR pitch angle and bulge fraction or Hubble type. Seigar et al. (2005) however reported a convincing connection between pitch angle in the NIR and the morphology of the galactic rotation curve, with open arms correlating with rising rotation curves, while pitch angles decline for flat and falling rotation curves.

The goal of this paper is to use the new measurements of the properties of the underlying *stellar* spiral arms from Paper I to re-examine the degrees to which the strengths and shapes of these arms are driven by the structural and environmental properties of their host galaxies. This is done mainly by examining correlations between the amplitude and pitch angles of the stellar arms with measures of galaxy morphology (independent of spiral structure) and mass, and with a measure of tidal perturbation from nearby companion galaxies. The same data are also used here to compare the shapes of the stellar arms with those traced by young gaseous and stellar components, and to constrain the degree to which the response of the gas discs and the local star formation rates are influenced by the amplitude of the spiral perturbation in the stellar discs.

The data and methods used in this work are described in detail in Paper I. A brief summary is as follows; 3.6 and 4.5  $\mu\text{m}$  NIR data from the *Spitzer* Infrared Array Camera (IRAC) are used in conjunction with complementary optical data in order to trace the stellar mass. In addition, IRAC 8  $\mu\text{m}$  data are used to trace the gas response, with particular emphasis on shocks. The data were analysed using azimuthal profiles (defined from fitting isophotal ellipses to the axisymmetric components of the galaxies) or radial profiles in the case that difficulties were encountered using azimuthal profiles. Azimuthal profile data were further examined by calculating the Fourier components in order to examine the amplitude and phase of individual modes, particularly the  $m=2$  component. This Fourier analysis was not possible for radial profile data; instead the total amplitude and phase were analysed. In this paper we consider only the 13 galaxies that constituted the so-called ‘detailed sample’ discussed in Paper I. We list various properties of these galaxies (which we go on to correlate with the properties of their spiral structure) in Table 1. The methods developed to isolate, identify, and parametrise the massive stellar arms are not well suited to strongly barred galaxies (which can distort arm shapes very significantly from a logarithmic shape), so this paper focuses mainly on normal and weakly barred galaxies; the role of bars in spiral structure is another important question awaiting further study (see Elmegreen et al. 2011).

## 2 THE RELATIONSHIP BETWEEN GALACTIC PROPERTIES AND THE NATURE OF SPIRAL STRUCTURE.

Previous studies in the optical and infrared have found conflicting trends relating the properties of spiral features with a range of galactic parameters such as Hubble type, galaxy mass and rotation curve morphology. This section sets out the findings from this work and discusses them in the context of previous results.

### 2.1 Amplitude and radial extent of spiral structure

Figure 1 presents data on the relative amplitude of the  $m=2$  component at 3.6  $\mu\text{m}$  as a function of radius. The axisymmetric components used to normalise the  $m=2$  components contain contributions from the disc and bulge; the halo contribution is not included. In M81, the only galaxy where the halo contribution has been considered (Kendall et al. 2008), adding the halo to the axisymmetric components makes very little difference to the relative amplitude, although this is not necessarily true in all cases. Data is presented for the 8 galaxies in the ‘detailed’ sample for which it was possible

Galaxy	HT	EC	$v_{flat}$	C	$\log(M_*)$	$A/\omega$	gf	SSFR
NGC 0628	Sc	9	217	2.95	10.1	0.39	0.32	$6.4 \times 10^{-11}$
NGC 1566	Sbc	12	196	3.57	10.7	0.55	0.18	-
NGC 2403	Scd	4	134	3.16	9.7	0.36	0.39	$7.6 \times 10^{-11}$
NGC 2841	Sb	3	302	3.27	10.8	0.48	0.17	$1.2 \times 10^{-11}$
NGC 3031	Sab	12	229	3.91	10.3	0.58	0.04	$2 \times 10^{-11}$
NGC 3184	Scd	9	210	2.40	10.3	0.21	0.22	$4.5 \times 10^{-11}$
NGC 3198	Sc	9	150	2.54	10.1	0.21	0.51	$7.4 \times 10^{-11}$
NGC 3938	Sc	9	196	2.95	10.1	0.41	0.39	$9.5 \times 10^{-11}$
NGC 4321	Sbc	12	222	3.03	10.9	0.36	0.21	$6.9 \times 10^{-11}$
NGC 4579	Sb	9	288	3.92	10.9	0.41	0.06	$1.1 \times 10^{-11}$
NGC 5194	Sc	12	219	3.0	10.6	0.55	0.125	$7.8 \times 10^{-11}$
NGC 6946	Sd	9	186	2.83	10.5	0.27	0.25	$1.0 \times 10^{-10}$
NGC 7793	Sb	2	115	2.48	9.5	0.22	0.29	$7.4 \times 10^{-11}$

**Table 1.** The properties of the galaxies analysed. The columns denote Hubble Type (HT), Elmegreen Class (EC), galactic rotation velocity (in  $\text{km s}^{-1}$ ) in flat portion of rotation curve, concentration (C), logarithm of total stellar mass, shear parameter ( $A/\omega$ ) of Seigar et al. 2005 (see Section 2.1.3), gas fraction (gf) and specific star formation rate (SSFR) in  $\text{yr}^{-1}$ .  $v_{flat}$ ,  $\log(M_*)$ , gf and SSFR are mainly derived from Leroy et al. (2008) as detailed in Sections 2.1.2, 2.1.3 and 2.1.4 respectively. C is derived from Bendo et al. (2007) (see Section 2.1.3 for definition).

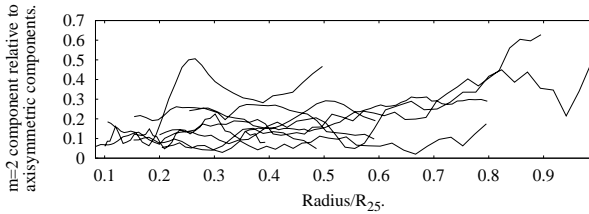


**Figure 1.** Relative amplitude of the  $m=2$  component of the  $3.6\mu\text{m}$  (stellar mass) data for all the ‘grand design’ spirals which could be analysed with Fourier components. Note this does not include data obtained from radial profiles. The data are shown for the radial range over which a logarithmic spiral could be traced.

to analyse azimuthal profile data and thus deduce the amplitude of various Fourier modes.

The galaxies with much less power in  $m=2$  are normally those in which there is no single dominant Fourier component and the power in modes  $m=1, 3$  and  $4$  is similar to that in  $m=2$  (these tend to be the optically flocculent galaxies like NGC 7793). The galaxy with a smaller radial range than many but a higher relative amplitude is NGC 1566.

In what follows we represent the ‘average’ amplitude of spiral structure in each waveband and for each galaxy as a straight average of the values obtained over the range of radii for which a logarithmic spiral pattern is detectable. These averages are listed for each galaxy in Table 2. Most galaxies thus have amplitudes in three bands (optical, IRAC1 and IRAC2) which are denoted by cross, dot and star symbols in each case. The data for each galaxy are linked by vertical lines. The larger symbols and dashed vertical lines correspond to the galaxies whose structure has been determined through radial profile analysis. The largest crosses denote the optical data for the three galaxies (NGC 3031, NGC 4321 and NGC 5194) which are apparently undergoing the strongest tidal interactions (i.e. with  $P > 10^{-3}$  (equation 1); see Table 4 and Figure 17). In almost all cases the main uncertainty is associated with the range of values at different radii (see Figure 1) and the issue of how datapoints at small and large radii should be weighted. The difference in mean amplitude between different wavebands is mainly due to the fact that in some galaxies the radial range over which

Galaxy	$\Delta_V$	$\Delta_{3.6}$	$\Delta_{4.5}$	$\Delta\phi_V$	$\Delta\phi_{3.6}$	$\Delta\phi_{4.5}$
NGC 0628	0.131	0.198	0.187	6.25	8.33	8.22
NGC 1566	0.247	0.284	0.287	3.92	4.50	4.57
NGC 2403	-	0.119	0.130	3.89	3.89	3.83
NGC 2841	-	0.069	0.076	2.85	2.85	3.60
NGC 3031	0.260	0.224	0.207	1.79	1.89	2.19
NGC 3184	0.225	0.282	0.304	6.57	5.55	5.49
NGC 3198	0.131	0.213	0.200	2.98	5.69	5.42
NGC 3938	0.091	0.093	0.086	5.01	4.49	4.37
NGC 4321	0.284	0.327	0.351	4.59	4.46	4.19
NGC 4579	0.177	0.188	0.166	3.06	3.50	3.76
NGC 5194	0.299	0.416	0.425	4.89	5.96	5.28
NGC 6946	0.166	0.214	0.222	1.97	1.56	1.55
NGC 7793	0.085	0.071	0.077	4.78	4.93	4.97

**Table 2.** The parameters of spiral structure in the visible,  $3.6\mu\text{m}$  (IRAC1) and  $4.5\mu\text{m}$  (IRAC2) bands:  $\Delta$  is the mean spiral amplitude (see text) and  $\Delta\phi$  is the total angle subtended by the arms in radians

a logarithmic spiral can be traced is different in different bands. The difference between amplitudes in different wavebands is therefore a measure of the uncertainty associated with radial averaging within the radial range studied (which is generally less than  $R_{25}$ ; see Figure 1). Note that in the case of galaxies that overlap with the sample of Elmegreen et al. (2011), the amplitude of variation at given radius is in good agreement between the two papers (once account is taken of the difference in the definition of arm contrast); the average values quoted in the Elmegreen et al. study are however generally higher due to the fact that the spiral structure is generally analysed out to larger radius. As noted above, in the bulk of our plots the vertical lines link average values in different wavebands; in order to avoid a confusing plethora of vertical lines we show the errors associated with radial averaging (as fine vertical lines) only in a single plot (Figure 4). The measurement errors for individual datapoints at given radius are generally much smaller than the uncertainties associated with radial averaging, being much less than 0.1 magnitudes in most of the azimuthal profile galaxies: see individual profiles and associated errors in Paper I.

### 2.1.1 Dependence on Hubble type and Elmegreen type.

We first plot the amplitudes of spiral structure as a function of Hubble type and Elmegreen type in Figures 2 and 3. There is no obvious correlation with Hubble type unless one excludes the three galaxies of type Sb and earlier. The correlation between spiral amplitude and Elmegreen class is much more evident: this is unsurprising since Elmegreen class is based purely on spiral morphology (albeit in the optical) with patchy, wispy spirals corresponding to arm class 1-4 and classes 5-12 corresponding to galaxies with increasingly prominent two armed grand design spiral structure. The fact that this classification scheme tracks the NIR amplitudes is a confirmation that the over-all level of spiral structure from galaxy to galaxy is reasonably well correlated in the optical and the NIR. We also note that the three ‘strongly interacting galaxies’ are associated with high Elmegreen class (i.e. well defined grand design structure).

These results are broadly consistent with those from an independent study by Elmegreen et al. (2011), based on Spitzer  $S^4G$  observations. In particular both studies show the absence of any correlation between arm amplitude and Hubble type when all spiral arm types are considered together, though Elmegreen et al. (2011) do see evidence for a possible correlation between arm-interarm contrast and Hubble type when flocculent galaxies are considered separately. Our observation of a correlation between arm amplitude and Elmegreen spiral type is also consistent with a trend observed in the Elmegreen et al. (2011) sample.

### 2.1.2 Dependence on galactic stellar mass and rotational velocity

Figures 4 and 5 plot the  $m=2$  amplitude against the galactic rotation velocity evaluated in the flat region of the rotation curve,  $v_{flat}$ , and the stellar mass  $M_*$ , with both these quantities being derived, where possible, from Leroy et al. (2008). Leroy et al. calculate  $v_{flat}$  by fitting the rotation curve with a function of the form  $v_{rot}(r) = v_{flat}(1 - \exp(-r/r_{flat}))$  where  $v_{flat}$  and  $r_{flat}$  are free parameters. For galaxies not included in the Leroy et al. sample, the same function is fit to the kinematic data from the sources given in Paper I, with errors estimated at the 10 per cent level. The stellar masses are calculated by integrating the galactic models produced by GALFIT (Peng et al. 2002) and applying the prescription to convert to stellar mass given in Leroy et al. (2008).

In both plots there is a clear trend for  $m=2$  average amplitude to increase with stellar rotation velocity and stellar mass, particularly if one excludes the three galaxies of Hubble type Sb or earlier. It should not be surprising that the trend is roughly the same in both plots since the Tully -Fisher relation (Tully & Fisher 1977) implies that  $v_{flat}$  is an approximate tracer of stellar mass. The same approximate trend was found by Elmegreen & Elmegreen (1987) who demonstrated that spiral arm amplitude is an increasing function of galaxy ‘size’ (proxied by the product of  $R_{25}$  and  $v_{flat}$ ). This trend is consistent with the decline in spiral amplitudes towards later Hubble types seen in Figure 2 since the general relationship between Hubble type and luminosity implies that later type galaxies are generally less massive. A qualitative correlation between the strength of spiral structure and parent galaxy luminosity has been recognised for decades (van den Bergh 1960a, b), and forms the basis of the van den Bergh luminosity classification of galaxies. The trends seen in Figures 4 and 5 can be regarded as a quantitative manifestation of this correlation. Figure 4 is particularly suggestive in that 11/13 of the galaxies appear to broadly follow a trend

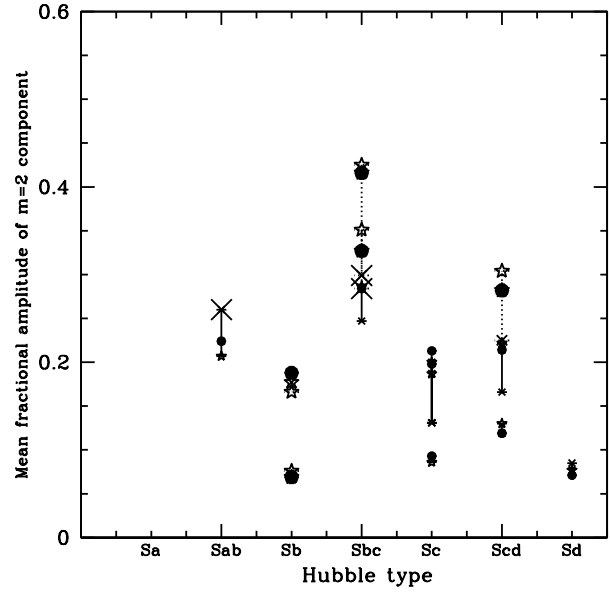


**Figure 2.** Average  $m=2$  relative amplitude plotted against Hubble type. The smaller symbols correspond to the 8 galaxies analysed with the azimuthal profile method, while the larger symbols denote the 5 galaxies analysed with radial profiles. Each galaxy has three data points shown, with separate amplitude estimates from  $3.6\mu\text{m}$ ,  $4.5\mu\text{m}$  and optical colour corrected data being denoted by dots, stars and crosses respectively; datapoints for a given galaxy are linked with vertical lines (dashed in the case of the radial profile galaxies). Note that for two galaxies (NGC 2403 and NGC 2841) no optical data are presented since these two galaxies were too flocculent in the optical to be able to extract reliable spiral parameters (see Paper I). The largest crosses denote optical data for the three galaxies with  $P > 10^{-3}$  (equation (1)) that are apparently undergoing tidal interactions (see Figure 17 and Table 4).

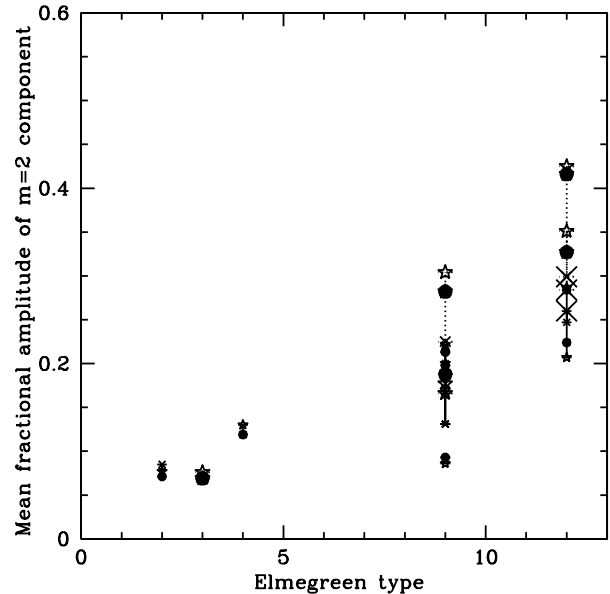


**Figure 3.** Average  $m=2$  relative amplitude plotted against Elmegreen class (see Figure 2 for explanation of symbols).

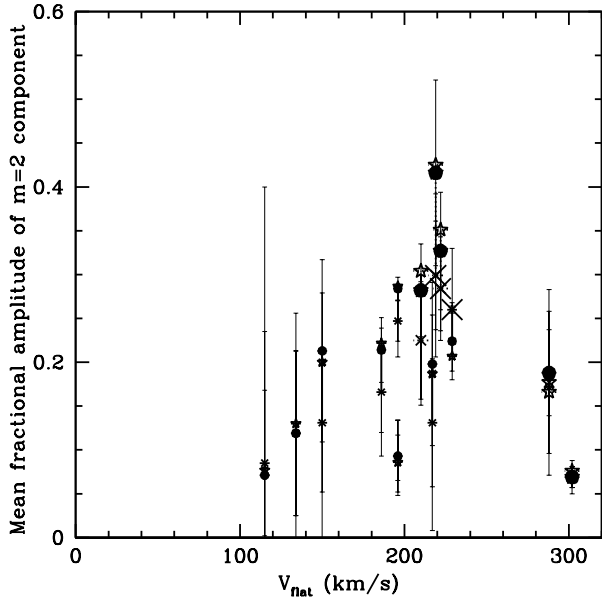


**Figure 4.** Average  $m=2$  relative amplitude plotted against magnitude of rotation velocity in the flat region of the rotation curve (see Figure 2 for explanation of symbols). The fine vertical lines (shown only in this plot for clarity) indicate the errorbars associated with radial averaging of the spiral amplitudes.

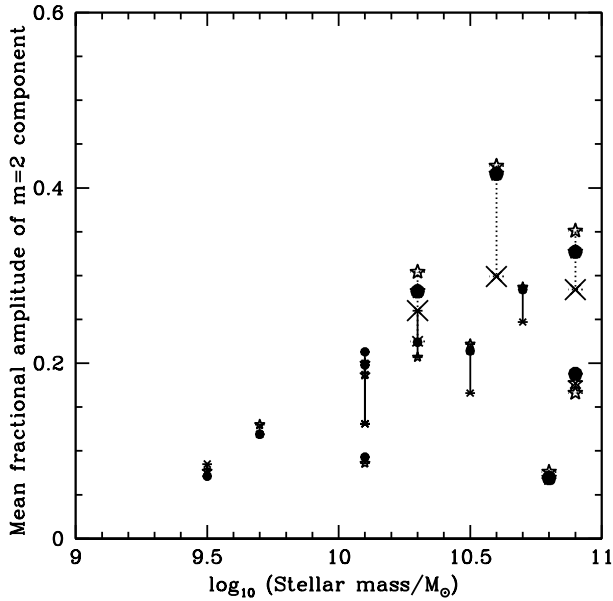


**Figure 5.** Average  $m=2$  relative amplitude plotted against galactic stellar mass (see Figure 2 for explanation of symbols).

of increasing amplitude of spiral features with increasing rotation velocity; the low amplitude of spiral features for the two objects with the largest rotational velocities (the Sb galaxies NGC 4579 and NGC 2841) are notably discrepant. We however caution against the drawing of any but the most tentative conclusions from this small sample.

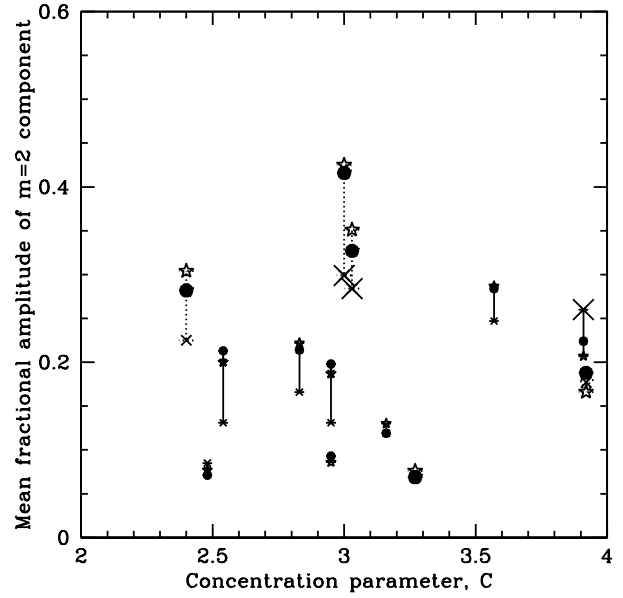


**Figure 6.** Average  $m=2$  relative amplitude plotted against concentration index (see Figure 2 for explanation of symbols).

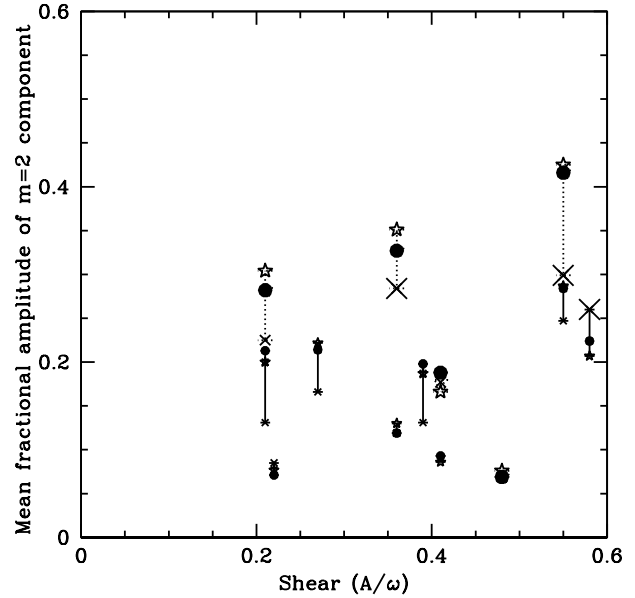


**Figure 7.** Dimensionless shear (see text) plotted against average  $m=2$  amplitude. Solid body rotation, flat rotation curves and falling rotation curves correspond to  $A/\omega$  values of 0, 0.5 and  $> 0.5$  respectively. See Figure 2 for explanation of symbols.

### 2.1.3 Dependence on concentration and galactic shear

Another factor which may influence the amplitude of spiral structure is the degree of central concentration of galaxies inasmuch as this affects the morphology of the galactic rotation curve. Komremdy & Norman (1979) argued that spiral waves are damped at the Inner Lindblad Resonance (ILR) and thus predicted that spiral structure (other than that driven by companions or bars) should be restricted to regions of galaxies with nearly solid body rotation

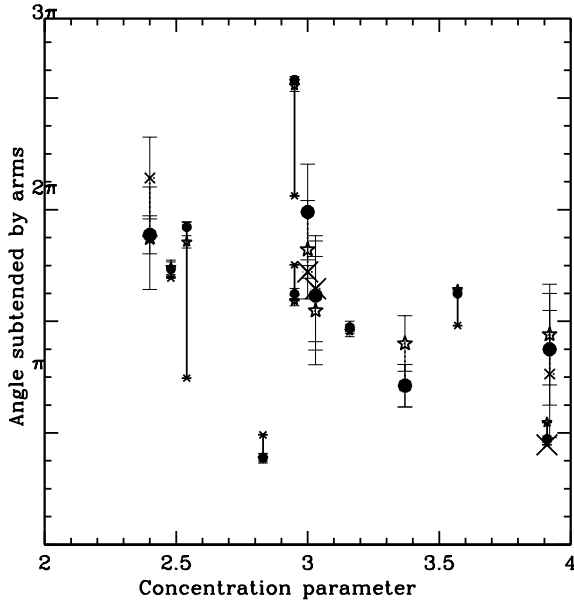


**Figure 8.** The concentration parameter plotted against angle subtended by the spiral arms (defined within the radial range of the logarithmic spiral). See Figure 2 for explanation of symbols.

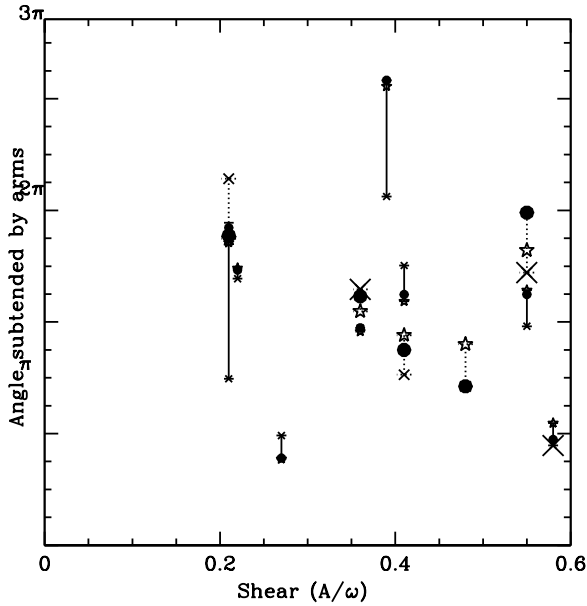


**Figure 9.** Dimensionless shear (see text) plotted against angle subtended by the spiral arms. See Figure 2 for explanation of symbols.

(for which there is no ILR). Their optical data showed some support for this hypothesis although this may be partly driven by the fact that low shear conditions favour more open spirals (which are more readily identified observationally). On the other hand this association between spiral structure and solid body rotation was *not* confirmed by the infrared study of Seigar et al. (2003) who found that spiral structure extends well beyond the region of solid body rotation. On a theoretical level, Sellwood & Carlberg (2014) have argued against the significance of ILRs for wave damping and indeed report a diminished amplitude of spiral structure in regions of

low shear (Sellwood & Carlberg 1984), ascribing this result to the relative ineffectiveness of swing amplification in conditions of low shear (Toomre 1981).

Here we investigate possible dependences on the rotation curve in two ways. We plot the amplitude of spiral structure against galaxy concentration parameter ( $C$ ) in Figure 6. We use the IRAC  $3.6\mu\text{m}$  concentration index ( $C$ ) data from Bendo et al. (2007), which is defined as the ratio of the radius containing 80 per cent of the light to that containing 20 per cent of the light, i.e.  $\frac{r_{80}}{r_{20}}$ . Higher values of  $C$  imply more concentrated emission and hence presumably also mass; the dynamical influence of a strong central mass concentration is to promote differential rotation (angular velocity declining with radius) and thus - according to the Kormendy & Norman argument - might be expected to be associated with lower amplitude spiral structure. Figure 6 however shows no evidence of an obvious (anti-)correlation between spiral amplitude and concentration index.

Figure 7 investigates the dependence of the strength of spiral structure on rotation curve morphology more directly, by evaluating for each galaxy the *dimensionless shear* defined by Seigar et al. (2005) as:  $\frac{A}{\omega} = \frac{1}{2} \left( 1 - \frac{R}{V} \frac{dV}{dR} \right)$  where  $A$  is Oort's constant,  $\omega$  is the angular velocity and  $V$  the local rotational velocity. In each case this quantity is evaluated for the region of the galaxy over which a spiral structure is detected. Since  $A/\omega$  is equal to  $-0.5 \times$  the power law index for the dependence of angular velocity on radius, it follows that solid body rotation corresponds to dimensionless shear of zero, a flat rotation curve to 0.5 and a falling rotation curve to larger values of  $\frac{A}{\omega}$ . The Kormendy & Norman hypothesis would preferentially associate prominent spiral structure with low values of the shear but Figure 7 shows no evidence for this.

The amplitude of the  $m=2$  component is only one measure of the strength of the spiral structure; another is the extent (radial or azimuthal) of the spiral arms. Seigar & James (1998) found 'a hint of a deficit' of galaxies with a large bulge to disc ratio and extended spiral arms, quantifying the latter in terms of the angle subtended by the arms. Figure 8 shows the angle subtended by the spiral arms plotted against concentration parameter for this sample (with the fine vertical lines representing the errorbars on the angle subtended), and provides some support for the Seigar & James result. However, if the angle subtended by the arms is plotted against dimensionless shear as shown in Figure 9, the trend is much less convincing, suggesting that disc shear is in fact not an important contributory factor to spiral arm extent. The mild (anti-) correlation between spiral arm extent and concentration parameter would then need an alternative explanation.

In summary then, we find no relationship between spiral arm amplitude or angle subtended by the arms with dimensionless shear and no relationship between spiral arm amplitude and concentration parameter. There is arguably a weak anti-correlation between the angle subtended by the arms and concentration parameter but this does not obviously relate to the rotation curve morphology.

#### 2.1.4 Dependence on gas fraction and specific star formation rate

The gas fraction is plotted against the relative amplitude of the  $m=2$  Fourier component in Figure 10. Where galaxies are not found in Leroy et al. (2008) the  $\text{HI}$  and  $\text{H}_2$  masses are taken from Kennicutt et al. (2003). For galaxies that are common to both datasets there is a scatter of up to 0.5 dex (but generally more like 0.2 dex) in gas masses.  $\text{H}_2$  masses are not given for NGC 1566 and NGC 3031: in these cases the total gas mass plotted is in fact only the  $\text{HI}$  mass.

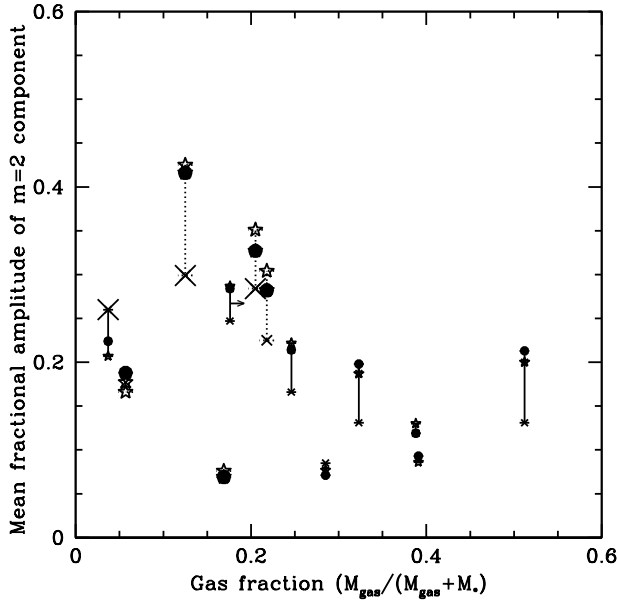


**Figure 10.** Gas fraction,  $(M_{\text{HI}+\text{H}_2})/(M_{\text{HI}+\text{H}_2} + M_*)$ , against average  $m=2$  relative amplitude. The arrow indicates that the gas fraction data for NGC 1566 give a lower limit (see Figure 2 for explanation of symbols).

NGC 3031 has very little detected CO, and so this should not be significant, but for NGC 1566 the difference may be larger: we indicate the fact that the gas fraction is a lower limit in this object via the arrow in Figure 10.

Figure 10 suggests a trend of decreasing amplitude of spiral arms with gas fraction (with again the three earliest type galaxies having discrepantly low spiral arm amplitude for their gas fraction values). This trend is in apparent contradiction to the notion that spiral structure is maintained by dynamical cooling provided by the continued production of stars from a dynamically cold gas reservoir. We also note that the three strongly interacting galaxies each lie at the top of the range of spiral amplitude at given gas fraction.

In Figure 11 we plot the  $m=2$  amplitude against specific star formation (normalised by the stellar mass). SFR data come from Leroy et al. (2008) except in the cases of NGC 3031 and NGC 1566: in NGC 3031 the SFR data derive from Perez-Gonzalez et al. (2006) and references therein. No SFR data are available for NGC 1566. We note that in principle a positive correlation between spiral arm amplitude and specific star formation rate could be driven by incomplete removal of young stellar emission from the NIR images.

However Figure 11 does not suggest any correlations between these quantities (in contrast to the mild positive correlation seen by Seigar & James 1998). This apparent lack of evidence for spiral structure enhancing the global SFR is discussed further in Section 4.2.

## 2.2 Pitch angles

The pitch angles are calculated by fitting a straight line to the data in the  $\phi$  vs  $\ln(R)$  plots presented in Paper I. The data from each galaxy and wavelength are presented in Table 3.

Possibly the first point that is worth commenting on is that, as was seen in Paper I, all these galaxies have phase-radius relationships that are close to logarithmic in nature ( $\phi \propto \ln(R)$ ) over at

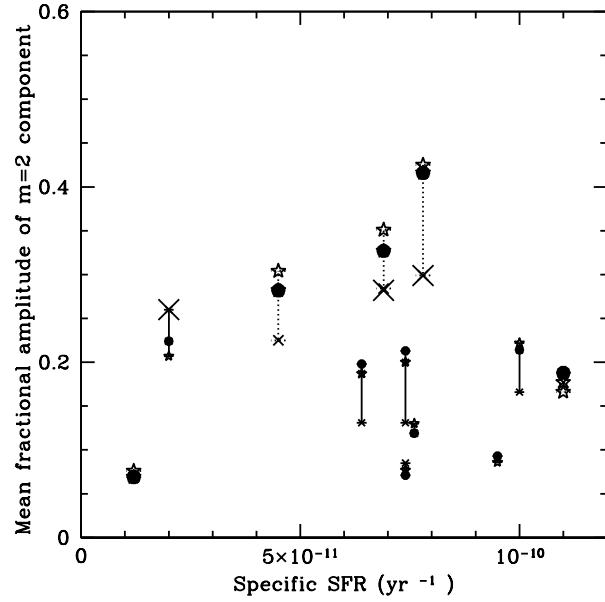


**Figure 11.** Average  $m=2$  amplitude plotted against specific star formation rate ( $\text{yr}^{-1}$ ). See Figure 2 for explanation of symbols.

Galaxy	Pitch angle ( $3.6\mu\text{m}$ , $4.5\mu\text{m}$ , optical)			method
NGC 0628	$16.2^{16.3}_{16.2}$	$16.4^{16.5}_{16.3}$	$17.3^{17.3}_{17.3}$	A
NGC 0628	$15.5^{16.5}_{14.6}$	$15.7^{16.7}_{14.8}$	$15.3^{16.5}_{14.2}$	R
NGC 1566	$19.7^{19.6}_{19.3}$	$19.4^{19.4}_{19.3}$	$22.3^{22.4}_{22.2}$	A
NGC 2403	$19.6^{19.8}_{19.3}$	$19.9^{20.1}_{19.6}$	-	A
NGC 2841	$6.7^{6.3}_{6.3}$	$6.5^{7.0}_{6.1}$	-	R
NGC 2841*	$9.4^{10.4}_{8.5}$	$8.1^{8.8}_{7.5}$	-	R
NGC 3031	$23.6^{23.9}_{23.3}$	$20.7^{20.7}_{20.7}$	$22.6^{22.7}_{22.6}$	A
NGC 3184	$19.5^{20.0}_{18.9}$	$19.9^{21.6}_{18.2}$	$18.2^{19.2}_{17.3}$	R
NGC 3198	$15.8^{15.8}_{15.4}$	$15.5^{15.7}_{15.4}$	$18.2^{18.2}_{17.8}$	A
NGC 3938	$15.0^{15.2}_{14.9}$	$15.4^{15.5}_{15.2}$	$17.8^{17.8}_{17.8}$	A
NGC 4321	$21.3^{23.7}_{19.4}$	$22.2^{24.8}_{20.1}$	$16.3^{18.0}_{14.8}$	R
NGC 4579	$20.3^{23.3}_{17.9}$	$16.6^{18.7}_{14.9}$	$17.9^{21.6}_{15.2}$	R
NGC 5194	$13.7^{14.7}_{12.8}$	$13.6^{14.8}_{12.6}$	$13.6^{13.8}_{13.5}$	R
NGC 6946	$29.3^{29.8}_{28.8}$	$29.5^{30.2}_{28.8}$	$24.0^{24.6}_{23.5}$	A
NGC 7793	$15.7^{15.9}_{15.5}$	$15.6^{15.8}_{15.4}$	$16.2^{16.3}_{16.1}$	A

**Table 3.** Measured pitch angles at  $3.6\mu\text{m}$ ,  $4.5\mu\text{m}$  and optical (V band). Method; this column lists the methods used to analyse the galaxy; A= azimuthal profiles, R=radial profiles. It is worth noting that the upper and lower bounds quoted in the Table result from accounting for statistical errors; the systematic errors (discussed in the text) may be larger, especially for highly inclined galaxies. \*NGC 2841; the first entry gives the pitch angle calculated for  $R > 0.45R_{25}$ , the second entry for  $R < 0.45R_{25}$  (the data used in the figures are those for  $R \geq 0.45R_{25}$ ).

least part of the disc of the galaxy. Although logarithmic spiral arms are predicted by QSSS theories (and subsequent related theories such as global spiral modes) this does not automatically lead to the conclusion that spiral arms must obey these relationships; that they do is notable. It is unlikely that this is merely a selection bias since the radial ranges for detectable spiral structure quoted throughout this work are not *defined* as regions of logarithmic spiral structure, even though this turns out to be the case in practice. There is one galaxy, NGC 2841 (pitch angle  $\sim 7^\circ$ ), for which the pitch angle should be treated with an extra degree of caution, because as de-

scribed in Paper I the high inclination and complex structure make the extraction of a single pitch angle problematical (see caption to Table 3). The errors quoted for all galaxies in Table 3 are the errors associated with accurately determining the phase of the  $m=2$  component in the Fourier fits or phase determined from radial profiles; these errors do not take into account the uncertainties in the galaxies' ellipticity or position angle. It is difficult to quantify the associated uncertainties in the pitch angle due to inaccuracies in galaxy orientation, although Block et al. (1999) found that by varying the inclination and position angle used to fit a highly inclined galaxy ( $i \geq 60^\circ$ ) the pitch angle could change by as much as 10 per cent. Nevertheless, it is striking that the pitch angles in the two infrared bands and optical (V) band are in general so similar to each other, with the differences being similar to the errors quoted in Table 3.

It is worth considering whether there is a systematic variation in pitch angle measured from the azimuthal profile and radial profiles. If anything, the radial method should produce pitch angles that are systematically smaller, due to measuring more of the contamination from young populations which are expected to be more tightly wound. The only galaxy for which a direct comparison is available is NGC 0628: the small difference (1 deg) is within the errors.

### 2.2.1 Comparison with previous ( $H\alpha$ and $K$ band) determinations

We now compare the pitch angles found in this work to results from optical ( $H\alpha$ ) data (Figure 12) for the set of 9 galaxies which overlap our sample and that of Kennicutt (1981). It can be seen that the late type spirals agree well, but that there is a systematic difference for the early types, Sab and Sb. The two galaxies that are most discrepant (NGC 3031 (Sab) and NGC 4579 (Sb)) are notably those that were shown in Paper I to exhibit the most convincing *offsets* between gas shocks and stellar density maxima. The sense of the offset (gas shock precedes stellar density maximum inward of corotation) combined with the fact that one would expect star formation to follow the shock after a fixed time (and therefore at an angular offset that decreases with radius for a differentially rotating galaxy) are both such as to explain smaller pitch angles in the  $H\alpha$  emission (assuming this traces recent star formation). Our sample size does not allow us to say whether this effect is a general feature of early type galaxies.

We can also compare some of our optical pitch angle determinations with those reported in the literature (see Ma 2001 and Davis et al. 2012: 7 members of our sample have B band pitch angle determinations also listed in either or both of these studies). As reported in the latter paper (Table 3) the agreement between our results and these other determinations is generally good (to within a few degrees or better in most cases).

Turning now to previous pitch angle determinations in the NIR we note that there is no overlap in sources between the galaxies listed in Table 3 and the galaxies previously studied in the K band by Seigar & James (1998) and Seigar et al. (2005). These two previous K band studies report rather different pitch angle distributions: Seigar & James 1998 record low values (generally in the 5–10 deg range) while the sample of Seigar et al. is broadly distributed in pitch angle, including a number of objects with  $i > 30$  deg. In that respect the latter distribution is similar to that found in the B and I band by Davis et al. (2012). Our own results follow a much narrower distribution (mainly lying in the range 15–20 deg in the optical as well as NIR bands). This result is most likely a consequence of our small sample size.

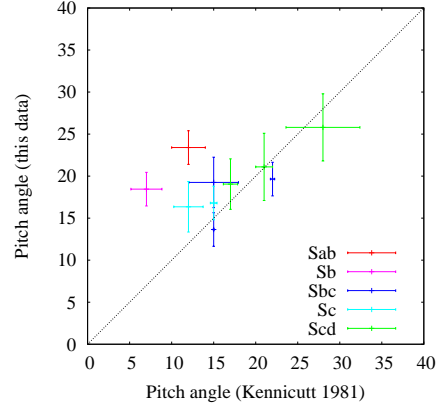


**Figure 12.** Pitch angles plotted against data from Kennicutt (1981) obtained using  $H\alpha$  data. The pitch angles of late type spirals are consistent (to within the errors). Early type spirals have systematically larger pitch angles measured in the NIR.

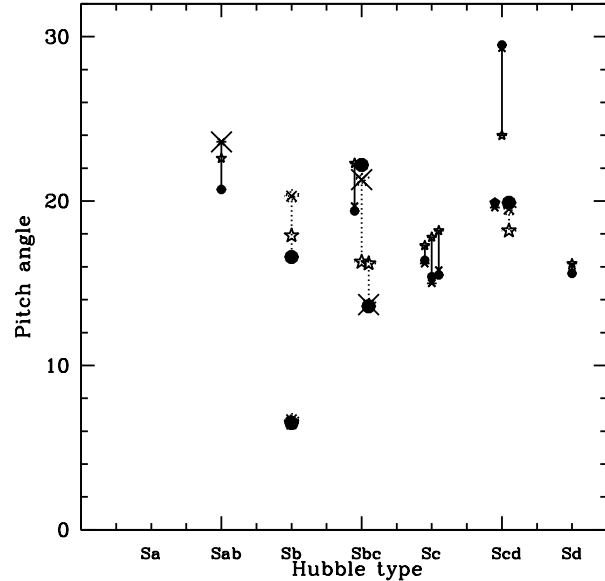
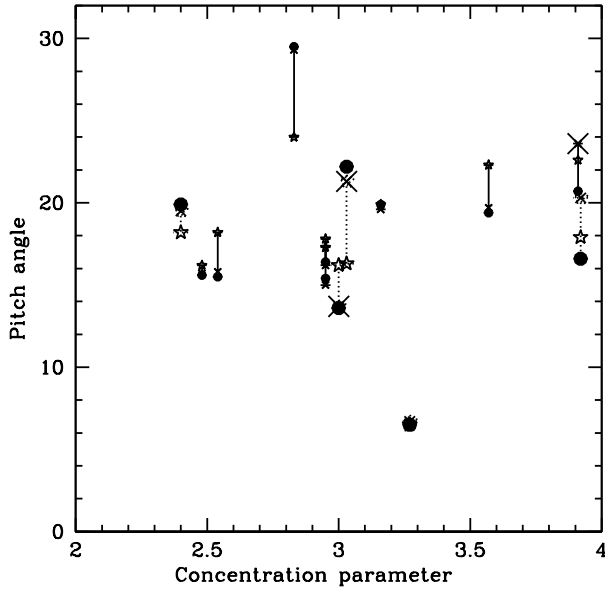


**Figure 13.** Pitch angles plotted against Hubble type. See Figure 2 for an explanation of the symbols

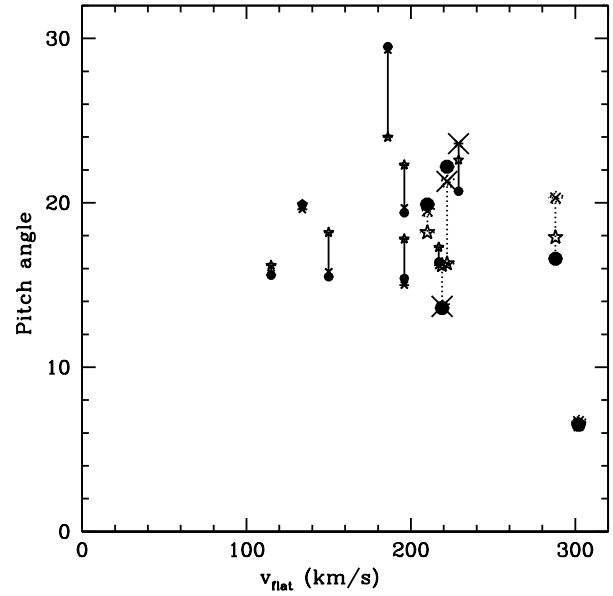
### 2.2.2 Dependence on Hubble type

Figure 13 plots the pitch angle of the  $m=2$  components from galaxies in the detailed sample against Hubble type. Roberts et al. (1975) proposed a relationship between Hubble type and pitch angle under the assumption that the latter is fundamentally a measure of bulge to disc ratio and using the dispersion relation of Lin & Shu (1964) to quantify the expectation that more loosely wound patterns are to be found in systems that are more disc dominated. The appearance of Figure 13 is strongly driven by the two galaxies with unusually large and small pitch angles in our sample (NGC 6941 and NGC 2841) and the fact that the former is of later Hubble type creates an impression of a correlation. However, the small range of measured pitch angles for the rest of the sample undermines the case for a correlation. Note that previous NIR results (Seigar & James 1998) also found no clear evidence of such a correlation (and again for the





**Figure 14.** Pitch angles plotted against mass concentration index  $C$ . See Figure 2 for an explanation of the symbols.



**Figure 16.** Pitch angles plotted against the magnitude of the rotation velocity in the flat portion of the rotation curve. See Figure 2 for explanation of symbols.

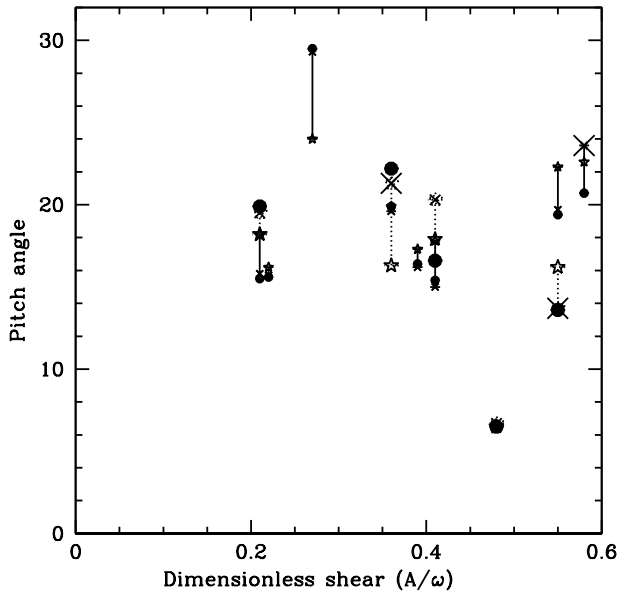


**Figure 15.** Pitch angles plotted against the dimensionless shear parameter. See Figure 2 for explanation of symbols.

reason that the bulk of objects in the sample were concentrated over a narrow range of pitch angles). Moreover the  $H\alpha$  study of Kennicutt (1981) found only a weak relationship between Hubble type and pitch angle (which is surprising given that the Hubble classification system implicitly considers the pitch angle of the spiral arms).

### 2.2.3 Dependence on rotation curve morphology and concentration.

Figure 14 shows likewise that there is no obvious relationship between pitch angles and central concentration, again contradicting the expectation that disc dominated systems should be associated with more open spiral patterns. This is consistent with the NIR results of Seigar & James (1998) and also with Kennicutt (1981) who found only a weak correlation with bulge to disc ratio. In Figure 15 we plot pitch angles against the dimensionless shear parameter of Seigar et al. (2005). These data show some weak evidence for more open structures in the case of galaxies with strongly rising rotation curves (although this impression is strongly driven by the two galaxies with outlying pitch angle values, NGC 2841 and NGC 6946). The relationship between pitch angles and galactic shear is much less evident than in the study of Seigar et al. (2005) and in particular we do not find the large pitch angles ( $i > 30$  deg.) at low shear ( $< 0.4$ ) that were reported in this work. An association between shear and pitch angle (in the sense found by Seigar et al.) is expected theoretically (Lin & Shu 1964, Bertin & Lin 1996, Fuchs 2000, Baba et al. 2013) and has recently been explored numerically by Grand et al. (2013) and Michikoshi & Kokubo (2014): these simulations show much larger pitch angles in the case of systems with rising rotation curves than we find here.

Finally, we plot in Figure 16 the dependence of pitch angle upon the galactic rotation velocity in the flat portion of the rotation curve (see Section 2.1.2). The appearance of an anti-correlation is strongly driven by one galaxy (NGC 2841) which combines a small pitch angle with a large rotational velocity, though as noted above the pitch angle in this case is particularly uncertain due to its large inclination and complex structure (Paper I). We thus find no evidence for the strong anti-correlation between pitch angle and  $v_{flat}$  that was found in the optical by Kennicutt & Hodge (1982).

### 2.2.4 Summary

The results presented in this section show no strong correlations between pitch angles and other galaxy parameters. The presence or absence of apparent correlations in Figures 13–16 need to be interpreted in the context of the fact that 11/13 of our galaxies have pitch angles within a rather narrow range, with only two galaxies having values that are either  $< 10$  deg or considerably greater than 20 deg (as such, our sample is almost all consistent with the predictions of swing amplification theory which predicts maximum pitch angles in the range 15 – 20 deg; Toomre 1981, Oh et al. 2008). However, as discussed in Section 2.2.1 above, we believe that this narrow range reflects the small sample size rather than differences in analysis method or the different range of wavebands employed compared with previous studies. Nevertheless the strongly bunched distribution means that the placing of the two most discrepant galaxies in each plot is a strong driver of whether there is an apparent correlation or not. With this caveat, we find no evidence to support the association between large pitch angles and rising rotation curves found by Seigar et al. (2005) in the near infrared, nor between large pitch angles low rotation velocities found by Kennicutt & Hodge (1982) in the optical.

We have also drawn attention to the suggestion that early type galaxies may be more tightly wound in  $H\alpha$  than in the near infrared. Finally, it is evident that the three strongly interacting galaxies do not occupy a distinctive region in Figures 13–16: clearly spiral structure that is driven by galaxy interactions cannot be distinguished from that in isolated galaxies on the grounds of near infrared pitch angle.

## 3 THE RELATIONSHIP BETWEEN GALACTIC ENVIRONMENT AND THE NATURE OF SPIRAL STRUCTURE

In the preceding plots we differentiated the three galaxies which we judge to be undergoing the strongest tidal interactions. Here we present the analysis of galactic environment that led us to this conclusion and examine how the strength of tidal interaction affects the amplitude of spiral structure.

We used the NASA/IPAC Extragalactic Database to search for companions to the 13 galaxies considered in this paper. The companions identified are detailed in Table 4 and all lie within  $\pm 400 \text{ km s}^{-1}$  of the target galaxy. The mass ratio was calculated using the relative  $B$  band magnitudes and assumed a constant mass-to-light ratio. Byrd & Howard (1992) proposed the tidal parameter  $P$  as a measure of the strength of galactic interactions:

$$P = \frac{M_c/M_g}{(r/R)^3} \quad (1)$$

where  $M_g$  is the galaxy mass,  $M_c$  the companion mass,  $R$  the galaxy radius, and  $r$  is the distance of closest approach. Byrd & Howard suggested a minimum value for  $P$  of 0.01 and 0.03 for pro- and retro-grade interactions respectively to induce a spiral response to the centre of the galaxy. In Paper I we analysed the incidence of ‘strong interactions’ (corresponding to galaxies with  $P$  values exceeding a given threshold) in the sample of galaxies that did and did not exhibit grand design spiral structure. We found that this incidence was only different (and higher in grand design spirals) if a threshold value of  $P = 0.01$  was adopted, thus confirming the estimate of Byrd & Howard regarding the value of  $P$  required for significant tidal perturbation of the galaxy.

Galaxy	Companion	$\frac{R_{proj}}{R_{25}}$	Relative mass	$P$
NGC 0628 +	UGC 01176	9.6	0.02	$2.2 \times 10^{-5}$
NGC 1566 +	NGC 1581	9.7	0.05	$5.5 \times 10^{-5}$
NGC 2403	NGC 2366	20.	0.1	$1.3 \times 10^{-5}$
NGC 2841	UGC 4932	6.1	0.01	$4.4 \times 10^{-5}$
NGC 3031 +	M82	2.7	0.28	$1.4 \times 10^{-2}$
NGC 3184	KHG 1013+414	7.4	0.01	$2.4 \times 10^{-5}$
NGC 3198	*	*	*	$5.5 \times 10^{-5}$
NGC 3938	-	-	-	-
NGC 4321 +	NGC 4323	1.4	0.01	$3.4 \times 10^{-3}$
NGC 4579 +	NGC 4564	9.8	0.25	$2.6 \times 10^{-4}$
NGC 5194 +	NGC 5195	0.8	0.25	$4.9 \times 10^{-1}$
NGC 6946	-	-	-	-
NGC 7793	-	-	-	-

**Table 4.** Values of  $P$  together with list of companions, mass ratios and normalised separations taken from the literature for all galaxies with a companion contributing  $P > 10^{-5}$  (the 6 galaxies marked with a + sign are those that were deemed to be interacting according to the ‘inclusive’ definition of Paper I: see text for details). \* In the case of NGC 3198 there are two galaxies (SDSS J 101848.78+452137.1 and VV 834 NEDOR) that contribute nearly equal  $P$  values and the quoted value is the sum of these.

Whereas in Paper I we assessed companions down to a limiting magnitude of  $B = 15$  and such that they lay within 10 scale-lengths ( $\frac{R_{proj}}{R_{25}} < 10.0$ ) of the main galaxy, this criterion did not correspond to a fixed  $P$  value (the 6 galaxies in our sample that had companions conforming to this criterion are marked with a + symbol in Table 4). In the present paper our focus is to discover whether (*within the sample of grand design spirals*) there is a significant correlation between the tidal parameter  $P$  and the amplitude of spiral structure. Accordingly we examine all the companions in the correct velocity range lying within 20 scale lengths and evaluate the maximum  $P$  value that is contributed by any of the companions. The mass ratios, normalised distances and  $P$  values are listed in Table 4 and  $P$  is plotted against spiral amplitude in Figure 17. We see that most of the sample have  $P$  values of around  $10^{-5}$  and indeed we found in Paper I that such values are also typical of the sample in which grand design spiral structure was not detected. We also note that a difficulty in relating the observed  $P$  value to the importance of tidal interactions: while the projected distance may be a substantial under-estimate of the three-dimensional separation, spiral structure is likely to reflect the strength of the interaction at a previous pericentre passage and thus the projected separation is in this sense an over-estimate of the relevant value.

Despite these caveats, Figure 17 demonstrates that the amplitude of spiral responses does indeed correlate positively with the tidal  $P$  parameter (in fact Figure 17 shows a more convincing correlation than any of the other plots we present here). The fact that 3/13 galaxies have  $P < 10^{-5}$  and yet display a significant spiral pattern implies that tidal interaction is *clearly not a pre-requisite* for inducing spiral structure (and indeed we have seen in Paper I that at least half the sample of galaxies without detected grand design structure have  $P$  values of  $10^{-5}$  or above). On the other hand, Figure 17 presents convincing evidence that where there is strong interaction the *amplitude of spiral structure is enhanced*. We have seen that the pitch angles of such ‘induced’ spirals are indistinguishable from spiral patterns in apparently isolated galaxies. We have also seen that where we have tentatively identified trends in the amplitude of spiral features (i.e. the positive correlations with  $v_{flat}$  and stellar mass shown in Figures 4 and 5 and the mild anti-

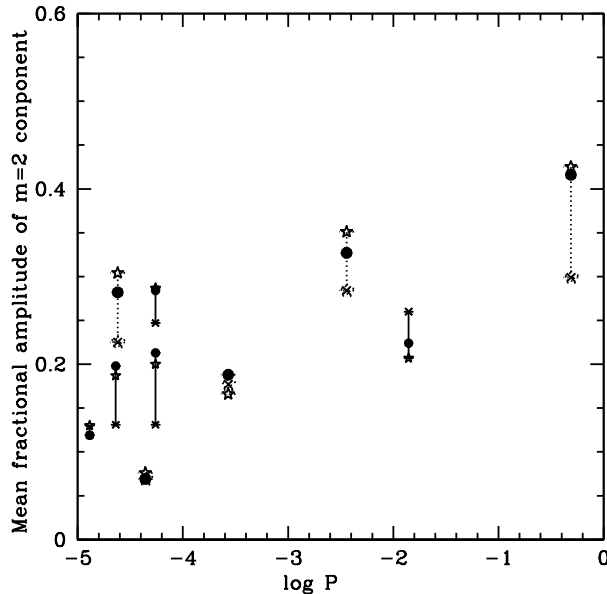


**Figure 17.**  $P$  (see equation (1) plotted against  $m=2$  relative amplitude.  $P$  gives a measure of the tidal interaction between two galaxies, and correlates strongly with the strength of the spiral. The galaxies with the largest  $P$  values (NGC 5194, NGC 3031 and NGC 4321 in descending order) are marked with the large crosses in the other Figures.

correlation with gas content shown in Figure 10) then the strongly interacting galaxies (i.e. those with  $P > 10^{-3}$ ) roughly follow these trends but at enhanced amplitude. Once again, we however caution against over-interpretation given our limited sample size.

#### 4 THE RESPONSE TO STELLAR SPIRAL STRUCTURE: GASEOUS SHOCKS AND ASSOCIATED STAR FORMATION.

The first half of this paper studied the effects of galaxy type, morphology and environment on the stellar spiral structure. However, as well as being influenced by the galaxy, a global spiral is expected to influence the galaxy in which it is located. The following section considers the effect of the spiral on the structure of the gas and the distribution of star formation in galaxies.

##### 4.1 Gas response

###### 4.1.1 Azimuthal offsets in the location of spiral shocks

Here we briefly recapitulate the results of Paper I with regard to the location of shocks in the gaseous component (as traced by  $8\mu\text{m}$  emission) with respect to the spiral in the stellar mass density (as traced at  $3.6\mu\text{m}$ ). Of the 13 galaxies in the detailed sample considered here, 4 galaxies (NGC 2403, NGC 2841, NGC 6946, NGC 7793) exhibited a flocculent response at  $8\mu\text{m}$  so it is not possible to talk meaningfully about the azimuthal alignment between the spirals manifest in the gas and the stars. Amongst the remaining 9 galaxies there is a general tendency for the  $8\mu\text{m}$  spiral to be located on the trailing (concave) side of the stellar ( $3.6\mu\text{m}$ ) spiral, i.e.

(at radii inwards of corotation) being *upstream* of the stellar spiral. Moreover the  $8\mu\text{m}$  spiral is generally somewhat more tightly wound. This is most clearly demonstrated in the case of NGC 3031 (M81) where the azimuthal offset increased systematically with radius and whose behaviour was the subject of detailed analysis in Kendall et al. 2008. Four other galaxies (NGC 3184, NGC 3198, NGC 3938 and NGC 4579) also demonstrated evidence of a systematic increase of offset angle with radius. In the remaining cases, the scatter in azimuthal offset is sufficiently large to prevent the identification of an obvious radial trend.

The possible significance of an upstream azimuthal offset between the shock in the gas and the maximum stellar density is discussed in Kendall et al. 2008. A scenario that predicts such an offset (with magnitude increasing with radius) is the case of a rigidly rotating spiral mode whose lifetime is sufficiently long to permit the gas to achieve a steady state flow in the imposed potential. In this case the solutions of Roberts (1969) and Shu et al. (1972) predict that the gas shocks upstream of the gas inwards of corotation, with the magnitude of this offset increasing with radius, a result that has been verified through hydrodynamic simulations (Gittins & Clarke 2004). Kendall et al. (2008) used these results to infer the corotation radius in NGC 3031 and obtained a value that is in reasonable accordance with other estimates in the literature. On the other hand, Clarke & Gittins (2006) and Dobbs & Bonnell (2008) undertook hydrodynamic simulations of gas in the case that the stellar potential derived from a high resolution re-simulation of the N-body calculations reported in Sellwood & Carlberg (1984). Notably in these simulations with a ‘live’ galactic potential, the gas shocks tended to trace the regions of instantaneous maximum stellar density and exhibited no systematic azimuthal offset with respect to the stellar spiral. A clear difference between this simulation and the idealised case involving a single long lived spiral mode is that, in the N-body calculations, spiral features come and go on a timescale of a few orbits. Clarke & Gittins related the gas morphology in this case to the fact that the gas did not have time to adjust to a steady state configuration on the timescale on which individual spiral features established and dissolved. In the case of spiral structure induced by a strong galactic encounter (as in the modeling of M51 - NGC 5194 - by Dobbs et al. 2010) no azimuthal offset was found between the gas and stellar spirals.

How do these theoretical results relate to the range of results that we find in our sample? We can divide our sample (as detailed above) into 4 galaxies with flocculent  $8\mu\text{m}$  structure, 5 with evidence for a systematic upstream offset with magnitude broadly increasing with radius and the remaining 4 as having no simple offset pattern (we denote these groups F(locculent), R(egular) and C(omplex): see Paper I for the phase diagrams on which this classification is based. We find no systematic differences between the galactic properties in these three groups apart from the fact that all the galaxies in the F(locculent) category are isolated ( $P < 10^{-5}$ ; see Table 2); the R(egular) and C(omplex) galaxies occupy a wide range of  $P$  values, although notably the galaxy which is undergoing by far the strongest interaction (NGC 5194) is in the C(omplex) category, in line with the simulations of this encounter by Dobbs et al. (2010).

We conclude from this that many of the isolated galaxies exhibit the kind of gas response seen in simulations based on live galactic potentials and that the most strongly interacting galaxy

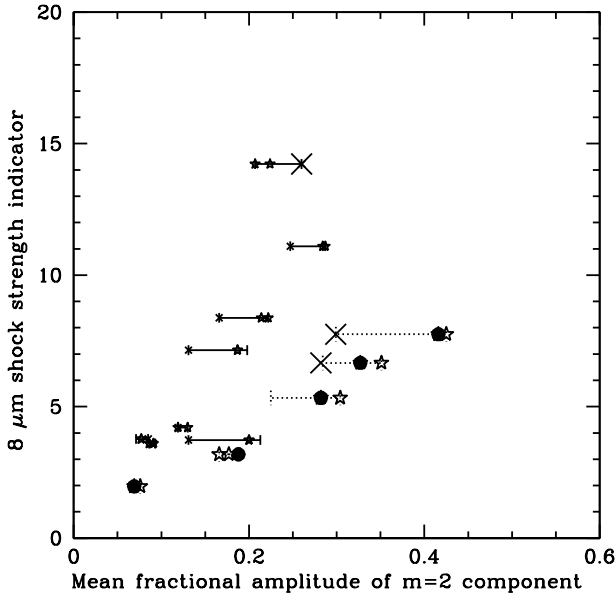


**Figure 18.** The  $8\mu\text{m}$  gas shock strength indicator (defined as the average of the four highest peaks in the  $8\mu\text{m}$  profile in the ‘on’ arm region, normalised by the average value of the  $8\mu\text{m}$  profile in the ‘off’ arm region) plotted against average  $m=2$  amplitude at  $3.6\mu\text{m}$ . See Figure 2 for an explanation of the symbols.

also agrees with simulations inasmuch as it exhibits no clear offset; the R(egular) group however exhibit a trend suggestive of a more long lived spiral pattern. We re-emphasise that this group is heterogeneous in terms of its galactic properties. To date there has been no detailed quantitative study of how tightly the offset data can be used to constrain the lifetime and nature of spiral structure in simulations.

#### 4.1.2 The strength of the shock as traced by $8\mu\text{m}$ emission

In addition to the position of the shock, it is instructive to look at the strength of the gas shocks as a function of the strength of the stellar spiral, since a larger spiral amplitude is expected to trigger a larger shock. We compared these properties for all galaxies in the sample, not just those for which the offset work was carried out. In contrast to the stellar mass maps, the gas response cannot be normalised by an axisymmetric component, so instead we simply divide the  $8\mu\text{m}$  azimuthal profile into ‘on’ and ‘off’ arm regions; ‘on’ arm is defined as being angles  $\pm \frac{\pi}{4}$  of the  $m=2$  peaks (‘off’ arm is the other  $\pi$  degrees, in two arcs). The response is calculated by taking the ratio of the highest peaks in the ‘on’ arm region to the average ‘off’ arm flux. Note that we use azimuthal profile data for analysis of the  $8\mu\text{m}$  emission for all galaxies in the sample, including those whose amplitude at  $3.6\mu\text{m}$  is obtained through radial profile analysis.

Figure 18 shows the trends in the gas response as a function of  $m=2$  amplitude and show that, as expected, the gas response will tend to be stronger for a larger stellar wave amplitude. (Note that we expect such a correlation to be weakened somewhat by the fact that  $8\mu\text{m}$  PAH features may be depleted by the strong UV emission associated with the enhanced star formation in shocked gas.)

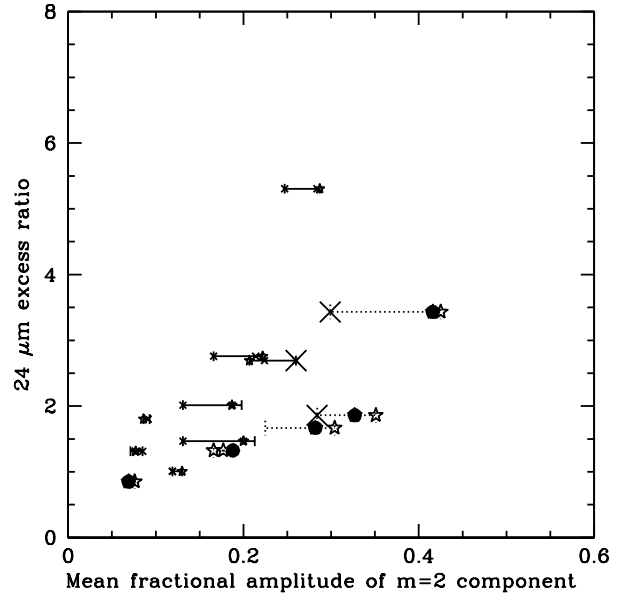


**Figure 19.** The  $24\mu\text{m}$  excess ratio (see text for definition). See Figure 2 for an explanation of the symbols.

#### 4.2 Star formation.

In this section we apply the same method as in Section 4.1.2 to define ‘on’ and ‘off’ arm regions, using the *Spitzer* MIPS (Rieke et al. 2004)  $24\mu\text{m}$  wavelength as a tracer of star formation (Calzetti et al. 2007).  $24\mu\text{m}$  emission is dominated by reprocessed radiation from young massive stars as demonstrated by its excellent spatial correlation with other diagnostics associated with such stars (see Relano & Kennicutt 2009 for such a demonstration in the case of  $\text{H}\alpha$  emission in M33). Helou et al. (2004) argued that the stellar continuum contributes at most a few per cent at  $24\mu\text{m}$ .

In Figure 19 we plot the ratio of the *excess* emission at  $24\mu\text{m}$  in the arm compared with the inter-arm region (where the excess is defined as the mean emission levels in that region minus the minimum emission level in that radial ring; note that in the case of the  $8\mu\text{m}$  data this minimum level is essentially zero in many regions and so in contrast Figure 18 presents the ratio of unsubtracted values.)

Figure 19 is qualitatively similar to Figure 18 and shows a clear dependence of the star formation response (as measured at  $24\mu\text{m}$ ) and the amplitude of variations in the stellar potential. The levels of contrast can be used to interpret Figure 11, noting that the dispersion in specific star formation rates and in the  $24\mu\text{m}$  excess ratios are comparable. This suggests that strong spiral structure can contribute significantly to the dispersion in specific star formation rates in our sample. Nevertheless, it cannot be the only driver since there are some notable counter-examples (for example, NGC 3031 with its strong  $24\mu\text{m}$  excess ratio and low specific star formation rate).

#### 5 CONCLUSIONS

By far the strongest correlation that we have identified (Figure 17) is between the *amplitude* of spiral structure and the strength of tidal

interaction as measured by the  $P$  parameter (equation (1)). We conclude - in line with our conclusions in Paper I - that a close tidal encounter appears to be a sufficient but not necessary condition for prominent spiral features. NGC 3198 is a good example of a galaxy that is unbarred and isolated and yet shows the ‘grand design structure’ that permits its inclusion in the detailed sample studied in this paper. Nevertheless, the amplitude of its spiral features is admittedly lower than the strongly interacting galaxies in our sample and moreover the  $m = 2$  mode is less dominant than in these galaxies.

We have indicated the galaxies with the three largest values of  $P$  (the strongly interacting galaxies) by the large crosses in all the other correlation plots. These galaxies are not atypical for the sample with regard to their pitch angles and the radial extent of spiral structure (as measured by the azimuthal angle subtended by the arms in Figures 8 and 9) and so do not strongly influence these plots. They are however all rather massive and gas deficient galaxies of type Sbc or earlier and we must therefore be mindful that apparent correlations may be driven by this association. This may be particularly relevant to the interpretation of Figures 4, 5 and 10.

Our sample covers a rather narrow range of pitch angles and it is thus unsurprising that we have not identified any correlations between pitch angles and other galactic parameters. Figure 12 may throw some light on previous comparisons between the pitch angles of spiral structure in the optical and NIR: for example in the most recent and sophisticated analysis of this issue by Davis et al. (2012) there is generally good agreement between pitch angles in the B and I bands. Discrepant galaxies have a tendency to have larger pitch angles at longer wavelengths. Figure 12 (which compares NIR pitch angles with pitch angles measured in  $H\alpha$ , an optical star formation indicator) suggests that in our sample a discrepancy of this sign is evident only for earlier Hubble types. This would suggest - if borne out in larger samples - that an association between early Hubble types and tightly wound arms may only be manifest in the optical (Clarke et al. 2010). In the most discrepant galaxies (NGC 3031 and NGC 4579) this difference in pitch angles can be explained by our previous demonstration (Kendall et al. 2008, 2011) that in these galaxies the spiral pattern traced at  $8\mu\text{m}$  in shocked gas is significantly displaced upstream with respect to the NIR (stellar) arms. In a differentially rotating galaxy it would then be expected that the spiral traced by star formation indicators should be more tightly wound than the stellar arms. The origin of azimuthal offsets is discussed in our previous papers; it is currently unclear whether there is a more general association between such offsets and galaxies of early Hubble type.

We also draw attention to the other strong correlation that we have found, i.e. the demonstration in Figures 18 and 19 of a clear dependence of the amplitudes of spiral structure in star formation ( $24\mu\text{m}$ ) and shock ( $8\mu\text{m}$ ) tracers on the amplitude of potential variations as traced in the NIR. The amplitude of spiral structure at  $24\mu\text{m}$  demonstrates that the star formation within the arms cannot on its own account for all the variation in specific star formation rate exhibited by the galaxies in our sample and there are indeed objects with strong arm contrast yet low specific star formation rates. However the range of arm amplitudes at  $24\mu\text{m}$  suggest that variation of strength of spiral features plays a significant contributory role in setting the specific star formation rates in disc galaxies.

## 6 ACKNOWLEDGMENTS.

Many thanks to Bob Carswell for much useful advice regarding the use of IDL, in particular the CURVEFIT program. We are indebted to Hans-Walter Rix for the idea of using colour-correction to make mass maps from optical data. Many thanks also go to Jim Pringle, Clare Dobbs, Stephanie Bush, Giuseppe Bertin and Jerry Sellwood for useful discussions over the course of this work and to Phil James and Marc Seigar for valuable observational input. We also thank the referee for constructive comments. This work makes use of IRAF. IRAF is distributed by the National Optical Astronomy Observatories, which are operated by the Association of Universities for Research in Astronomy, Inc., under cooperative agreement with the National Science Foundation.

## REFERENCES

- Baba, J., Saitoh, T., Wada, K., 2013. ApJ 763,46
- Bendo, G., Calzetti, D., Engelbracht, C. et al., 2007. MNRAS 380, 1313
- Bertin, G., Lin, C., 1996. in *Spiral structure in galaxies a density wave theory*, Publisher: Cambridge, MA MIT Press.
- Block D. L., Bertin G., Stockton A., Grosbol P., Moorwood A. F. M., Peletier R. F., 1994, A&A, 288, 365
- Block D. L., Bertin G., Stockton A., Grosbol P., Moorwood A. F. M., Peletier R. F., 1994, A&A, 288, 365.
- Block D. L., Puerari I., Frogel J. A., Eskridge P. B., Stockton A., Fuchs B., 1999, Ap&SS, 269, 5
- Block D. L., Wainscoat R. J., 1991, Nature, 353, 48
- Byrd G. G., Howard S., 1992, AJ, 103, 1089
- Calzetti, D., Kennicutt, R., Engelbracht, C. et al. , 2007. Ap J 666, 870
- Cepa J., Beckman J. E., 1990, ApJ, 349, 497
- Clarke, C., Gittins, D., 2006. MNRAS 371,530
- Clarke, C., Kendall, S., Kennicutt, R., 2010 in AIP Conf. Proceedings 1242,129
- Davis, B., Berrier, J., Shields, D. et al., 2012. ApJ S 199,33
- Dobbs C. L., Bonnell I. A., 2008, MNRAS, 385, 1893
- Dobbs, C.L., Theis, C., Pringle, J., Bate, M., 2010. MNRAS 403, 625
- Elmegreen D. M., Chromey F. R., Bissell B. A., Corrado K., 1999, AJ,118,2618
- Elmegreen D. M., Elmegreen B. G., 1984, ApJS, 54, 127
- 1987, ApJ, 314, 3
- Elmegreen, D.M. et al 2011, ApJ, 737, A32
- Fuchs, B., 2000. In *Dynamics of Galaxies from the Early Universe to the Present*, 15th IAP meeting, eds. Combes, F., Mamon, G., Charmandaris, V., p.53
- Gerola H., Seiden P. E., 1978, ApJ, 223, 129
- Gittins D. M., Clarke C. J., 2004, MNRAS, 349, 909
- Grand, M., Kawata, D., Cropper, M., 2013. A & A 553, A77
- Grosbol P., Patsis P. A., Pompei E., 2004, A&A, 423, 849
- Helou, G., Roussel, H., Appleton, P. et al., 2004. ApJS 154,253
- Kendall S., Kennicutt R. C., Clarke C., Thornley M. D., 2008, MNRAS, 387, 1007
- Kendall, S., Kennicutt, R., Clarke, C., 2011. MNRAS 414,538 (Paper I)
- Kennicutt, Jr R. C., Hodge P., 1982, ApJ, 253, 101
- 1981, AJ, 86, 1847
- Kennicutt Jr. R. C, 1998, ApJ, 498, 541
- Kennicutt Jr. R. C., Armus L., Bendo G., et al. 2003. PASP 115,928

- Kormendy J., Norman C. A., 1979, *ApJ*, 233, 539  
Leroy, A., Walter, F., Brinks, E., et al. 2008. *AJ* 136,2782  
Lin C. C., Shu F. H., 1964, *ApJ*, 140, 646  
- 1966, *Proceedings of the National Academy of Science*, 55,229  
Lindblad B., 1964, *Astrophysica Norvegica*, 9, 103  
Ma, J., 2001. *ChJAA*, 1, 395  
Michikoshi, S., Kokubo, E., 2014. *ApJ* 787,174.  
Mueller M. W., Arnett W. D., 1976, *ApJ*, 210, 670  
Oh S. H., Kim W.-T., Lee H. M., Kim J., 2008, *ApJ*, 683, 94  
Perez-Gonzalez P. G., Kennicutt Jr. R. C., Gordon K. D., et al.,  
2006. *ApJ* 648,987  
Relano, M., Kennicutt, R. Jr., 2009. *ApJ* 699,1125  
Rieke G. H., Young E. T., Engelbracht C. W., et al. 2004. *ApJ* S  
154,25  
Roberts, W. W., 1969, *ApJ*, 158, 123  
Roberts Jr. W. W., Roberts M. S., Shu F. H., 1975, *ApJ*, 196, 381  
Schweizer, F., 1976. *ApJS*, 31, 313  
Seigar M. S., Block D. L., Puerari I., Chorney N. E., James P.  
A., 2005, *MNRAS*, 359.1065  
Seigar, M., Bullock, J., Barth, A., Ho, L., 2006. *ApJ* 645,1012  
Seigar M. S., Chorney N. E., James P. A., 2003, *MNRAS*, 342, 1  
Seigar M. S., James P. A., 1998, *MNRAS*, 299, 685  
-, 2002, *MNRAS*, 337, 1113  
Sellwood, J., Carlberg, R., 1984. *ApJ* 282,61  
-, 2014. *ApJ* 785,137  
Sheth, K. et al. 2010, *PASP*, 122, 1397  
Shu, F., Millone, V., Gebel, W., Yuan, C., Goldsmith, D., Roberts,  
W., 1972. *ApJ* 173,557  
Thornley M. D., 1996, *ApJ*, 469, L45  
Toomre A., 1981, in *Structure and Evolution of Normal Galaxies*,  
Fall S. M., Lynden-Bell D., eds., pp. 111-136  
Tully R. B., Fisher J. R., 1977, *A&A*, 54, 661  
van den Bergh, S., 1960a, *ApJ* 131,215  
van den Bergh, S., 1960b. *ApJ* 131,558